Construction and Building Materials xxx (2010) xxx–xxx

Contents lists available at ScienceDirect

Construction and Building Materials

journal homepage: www.elsevier.com/locate/conbuildmat

Numerical simulation of elastic waves for visualization of defects

D.G. Aggelis [a,*], N. Tsimpris [a], H.K. Chai [b], T. Shiotani [c], Y. Kobayashi [d]

[a] Department of Materials Science and Engineering, University of Ioannina, 45110 Ioannina, Greece
[b] Research Institute of Technology, Tobishima Corporation, 5472 Kimagase, Noda-shi, Chiba 270-0222, Japan
[c] Graduate School of Engineering, Kyoto University, Nishikyo-ku, Kyoto 615-8540, Japan
[d] College of Science and Technology, Nihon University, 8-14, Kanda-Surugadai 1-chome, Chiyoda-ku, Tokyo 101-8308, Japan

ARTICLE INFO

Article history:
Received 16 May 2010
Received in revised form 30 July 2010
Accepted 23 August 2010
Available online xxxx

Keywords:
Concrete
Elastic waves
Non-destructive testing
Simulation
Tomography
Voids

ABSTRACT

Due to aging of civil infrastructure, non-destructive testing (NDT) is of continuously increasing significance. The ultimate aim is the detection of defects in the interior of a structure with the highest possible accuracy, in order to proceed to specific repair action. Pulse velocity tomography is a technique to visualize the interior. Using a number of pulsers and receivers for introduction and recording of the transient elastic wave at different points on the surface of a structure, a potentially dense network of interconnecting wave paths are examined as to their wave transit time. Each "cell" of the cross section is assigned a velocity value and the interior is visualized. However, the confirmation of the results is not always possible except for cases where the cracks are visible from the surface or in case specific model defects are placed during casting of specimens. In the present paper numerical simulations of wave propagation were conducted for different geometries. Different types of inhomogeneity were applied, such as voids, deteriorated zones, as well as steel reinforcing bars. The transit time information calculated in these cases, led to the corresponding tomograms. Based on the comparison between the actual geometry of the void and the tomograms, the accuracy of the technique is studied, as well as parameters to improve the testing, like applied excitation frequency and number of sensors.

1. Introduction

Due to aging of concrete structures, non-destructive testing (NDT) is becoming of increasing importance. The results can be considered in the process of maintenance in order to take the necessary repair action, extend the service life of the structures for a long period of time and contribute therefore, to the safe and economic infrastructure management. In certain cases NDT can act as warning against catastrophic failures. Different methods are applied, based on a variety of principles. However, there is one global goal concerning the inspection; visualization of the results. Techniques like X-rays, radar, thermography and elastic waves (ultrasonics) aim to produce "tomograms" of the structure [1–4] in order the results to be easily understood not only by the engineers but also by the owner of the structure.

Concerning ultrasonics, tomography has been used with success in various cases of large structures [5–7]. Due to the empirical correlations between pulse velocity and strength of concrete [1,8], valuable information can be exploited by a tomogram, where portions that exhibit velocity lower than 3500 m/s are considered of troublesome integrity, while portions with velocity higher than 4000 m/s are considered of acceptable quality. The tomograms can be stored in the structure's record and be compared with new ones after a period of years or after repair in order to estimate the repair effect [6,7]. In any case the level of the velocity indicates the general status of the material; however, the details of the existing defects cannot always be determined. Due to the size of the structures it is not always possible to validate the exact result unless special conditions apply, i.e. specific cracks break the surface at visible points [6,9] or in case specific model voids have been embedded in laboratory specimens with known geometry and location [10]. However, this is not always possible due to the large size of realistic concrete blocks as well as logistics.

In this paper numerical simulations are used in order to produce ultrasonic results for various cases of geometries and voids in order to conduct the corresponding tomograms, based on the travel time of the elastic waves through the thickness of the structure. Numerical simulations of wave propagation have been conducted for numerous cases, e.g. particulate and fibre composites [11,12] or concrete [13,14]. Numerical simulations offer certain advantages, as they allow fast and reliable results for a variety of cases which are costly and time-consuming to reproduce in actual experiment. Different parameters can be tested, such as experimental (adequate number of sensors, number of accessible sides of the structure, excitation frequency), structural parameters like

* Corresponding author. Tel.: +30 26510 08006; fax: +30 26510 08054.
E-mail address: daggelis@cc.uoi.gr (D.G. Aggelis).

0950-0618/$ - see front matter © 2010 Elsevier Ltd. All rights reserved.
doi:10.1016/j.conbuildmat.2010.08.008

the effect of different material zones or parameters concerning the performance of the tomography procedure itself (number of iterations, mesh size) in order to lead to higher accuracy and shorter computational time. The specific cases discussed herein concern some simple model voids, such as a central void in an elastic matrix in order to confirm the tomography capacity and compare the results with different excitation frequencies. Next, some cases of distributed damage in the form of deteriorated surface zones are addressed in order to test the procedure when none of the transducers is in contact to the healthy material. The existence of metal reinforcement can complicate ultrasonic assessment [15] and therefore, it was also studied in relation to the existing damage. Additionally, the access to two or four sides of the structure is also discussed.

2. Basic concept of travel-time tomography

The simplest form of ultrasonic testing employs a pulser–receiver configuration. They are placed on the same or opposite sides of a structure. When a pulse is introduced into the material, the time taken by the pulse to reach the receiver, defines the wave velocity of the material if the length of the wave path is known. In case a number of excitation and reception points are used, a dense pattern of wave paths is examined which is more representative of the whole volume. One of the basic concepts of tomography is the separation of the examined cross section with a rectangular mesh, see Fig. 1a. Depending on the size of the mesh, the various wave paths, pass through a number of cells. Each cell is initially assigned the average of the velocities of the wave paths passing through the specific cell (Fig. 1a). A brief description of the algorithm can be found below, while the interested reader is also directed elsewhere [16,17].

The travel-time tomography is a procedure to invert the travel time tabulated as a function of distance for the pulse velocity. Travel time is in fact an average of the inverse of velocity, or specifically identified as the "slowness" of a pulse travelling in a medium. Based on the ray theory, the travel time T between two points A and B is given by the path integral [18]:

$$T = \int_A^B \frac{1}{v} dl = \int_A^B s \cdot dl \tag{1}$$

where the integral follows the ray path from A to B with v as the velocity, s as the slowness and dl as the element length. The equation can be expressed in matrix form as [19]:

$$G(x) = b \tag{2}$$

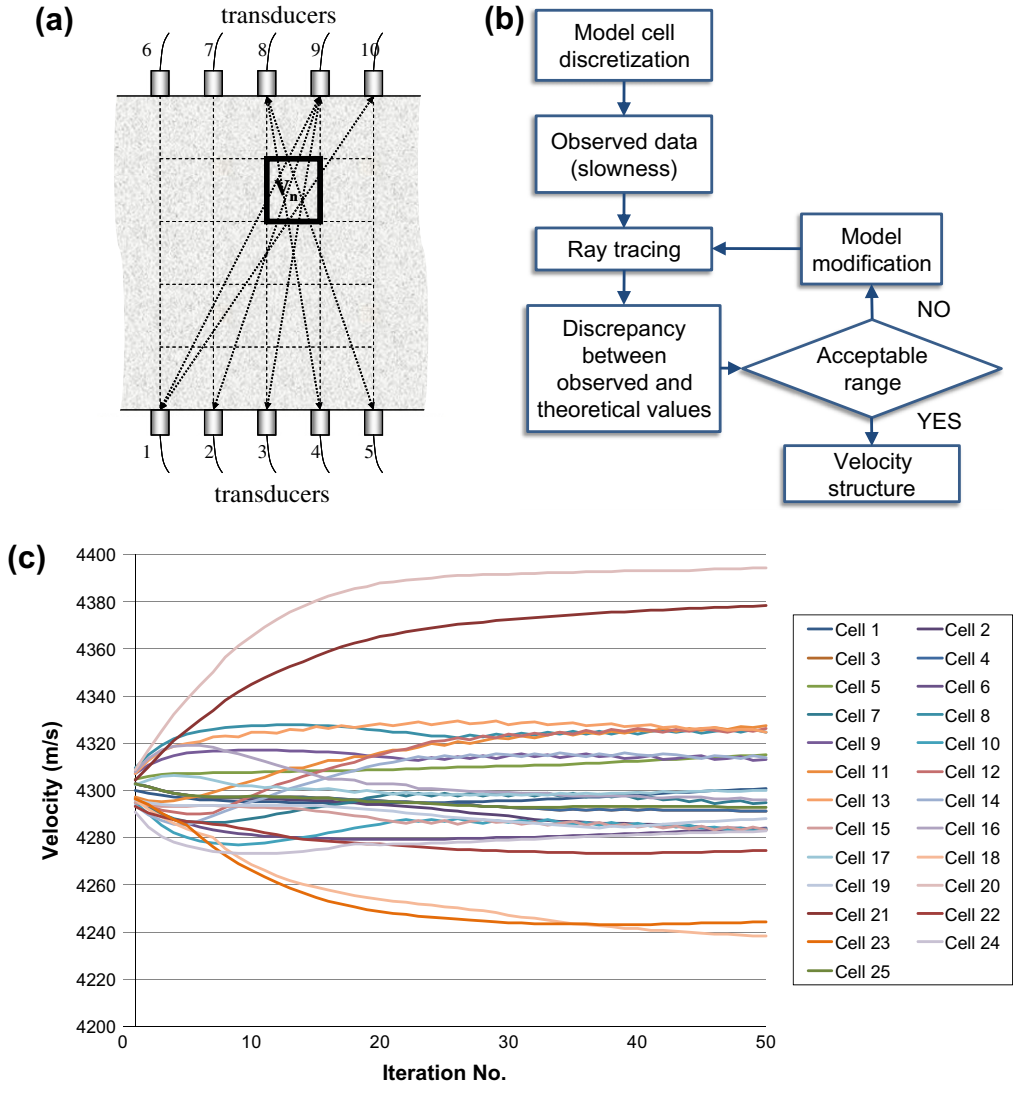

Fig. 1. (a) Mesh applied for a typical tomography, (b) procedure for travel-time tomography reconstruction and (c) convergence of velocity computation for different cells.

Please cite this article in press as: Aggelis DG et al. Numerical simulation of elastic waves for visualization of defects. Constr Build Mater (2010), doi:10.1016/j.conbuildmat.2010.08.008

where $G(x)$ is the integration operation with respect to x. For the travel-time tomography, x is the distribution of s in the model and b is the vector of travel time. The equation poses a continuous inverse problem because the data are a set of travel times between a set of pairs of points A and B, which are to be inverted for the model. Since the integral follows the ray path and the ray path depends on the slowness, the inverse problem is highly non-linear and has to be solved iteratively. The computation process is referred to as ray tracing. Common ray tracing procedures for tomography reconstruction include algebraic reconstruction techniques (ART) and simultaneous iterative reconstruction technique (SIRT). The rays are usually restricted to the edges of the mesh and therefore a weighted shortest path problem can be solved. Travel times are not always accurately estimated in the first few iterations because not every path can be used, or there is insufficient observed data. However, with increasing refinement in the computation, the discrepancy diminishes and the velocity of each element converge. The procedure for travel-time tomography reconstruction is depicted in Fig. 1b. In the specific case the number of iterations was set to 100, while as indicatively shown in Fig. 1c for examples of computation results of this study, satisfactory convergence was reached for all cells at less than 50 iterations.

3. Numerical simulation

In order to produce the raw data (travel times) to conduct tomography, numerical simulation software was used. The cases examined were solved numerically in order to produce the waveform of the receiver and extract the transit time of the wave. The fundamental equation governing the two-dimensional propagation of stress waves in a perfectly elastic medium, ignoring viscous losses is as follows:

$$\rho \frac{\partial^2 u}{\partial t^2} = \mu \nabla^2 u + (\lambda + \mu) \nabla \nabla \cdot u \tag{3}$$

where $u = u(x, y, t)$ is the time-varying displacement vector, ρ is the material density, λ and μ are the first and second Lamé constants, respectively, and t is time. The simulations were conducted with commercially available software [20], that solves the above equation using the finite difference method in the plane strain case. Eq. (3) is solved at discrete points with respect to the boundary conditions of the model, which include the input source that has predefined time-dependent displacements at a given location and a set of initial conditions [21]. For heterogeneous geometries like the ones studied herein, wave propagation in each distinct homogeneous phase is solved according to Eq. (3), while the continuity conditions for stresses and strains must be satisfied on the interfaces [21].

Materials were considered elastic without viscosity components. The mechanical properties of the different materials are shown in Table 1. In total four different types of materials were considered: concrete, deteriorated concrete, steel and voids (air). The basic geometry utilized was a square of 500 mm side (concrete matrix) on which the different inhomogeneities were incorporated as shown in Fig. 2a. The "pulser" was triggered by a displacement excitation of one cycle and the simulation was repeated for two different frequencies, namely 20 kHz and 200 kHz in order to estimate the effect of the different wavelengths (210 mm and 21 mm respectively). The "receivers" were placed on other sides of the geometry following a pre-defined pattern. One example of a geometric model of a homogeneous matrix is shown in Fig. 2a. The "receivers" provide the average vertical displacement over their length, meaning that the receiver signal represents the average response over a number of nodes. Therefore, after one excitation, a number of wave paths are examined, depending on the number of sensors on the opposite side (e.g. 6 for Fig. 2a). Consequently, the excitation is conducted by the adjacent pulsers in order to complete the examination of the required pattern of wave paths.

The simulation accuracy depends on the density of the points on which Eq. (3) is solved. Due to the large size of the examined geometry, too fine mesh would increase the calculation time making simulations impractical. Thus, preliminary simulations were conducted on a specific geometry to estimate the effect of mesh size on accuracy as well as computation time. Specifically simulations were conducted on the diagonal path in a geometry containing a circular inhomogeneity, and two vertical zones of lower stiffness (Fig. 2b). They showed that reducing the mesh size, influences the calculated transit time, and therefore, pulse velocity, as seen in Fig. 2c. Using curve fitting, for infinitely small mesh size, the transit time for the diagonal path of Fig. 2b is projected to 183.36 μs. Using a mesh size of 30 mm although the simulations were conducted very quickly, the deviation compared to the projected value is almost 3%. Using the mesh size of 4 mm the deviation is 0.57% while the simulations were conducted in a timely manner. Therefore, the mesh size of 4 mm was considered adequate and used throughout the whole

Table 1
Mechanical properties of the model materials.

Material	λ (GPa)	μ (GPa)	ρ (kg/m^3)	E (GPa)	ν	C_p (m/s)
Concrete	11.1	16.6	2500	40	0.2	4216
Air	10^{-4}	10^{-6}	1.2	3×10^{-6}	0.499	300
Deteriorated concrete	6.9	10.4	2500	25	0.2	3333
Steel	121	81	7800	209	0.29	6023

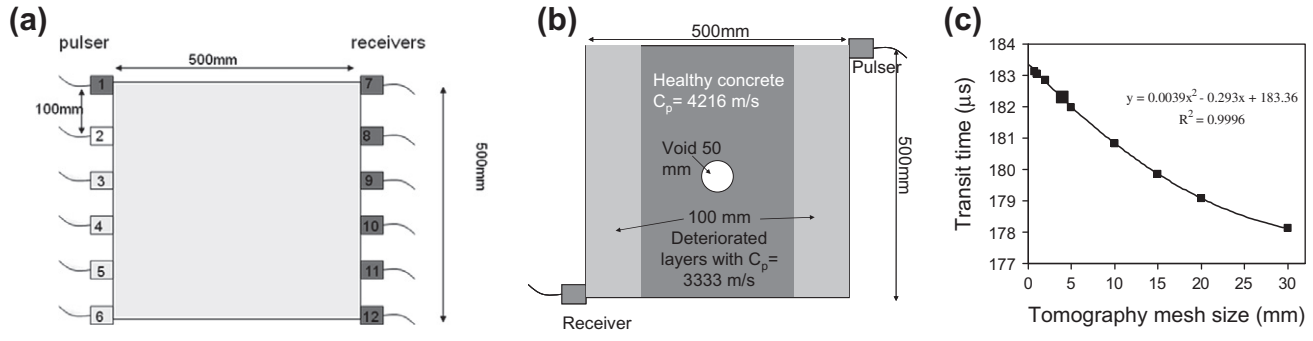

Fig. 2. (a) Typical geometry and sensor arrangement, (b) model with surface deterioration zones and central void and (c) transit time vs. tomography cell size for the geometry of Fig. 2b.

Please cite this article in press as: Aggelis DG et al. Numerical simulation of elastic waves for visualization of defects. Constr Build Mater (2010), doi:10.1016/j.conbuildmat.2010.08.008

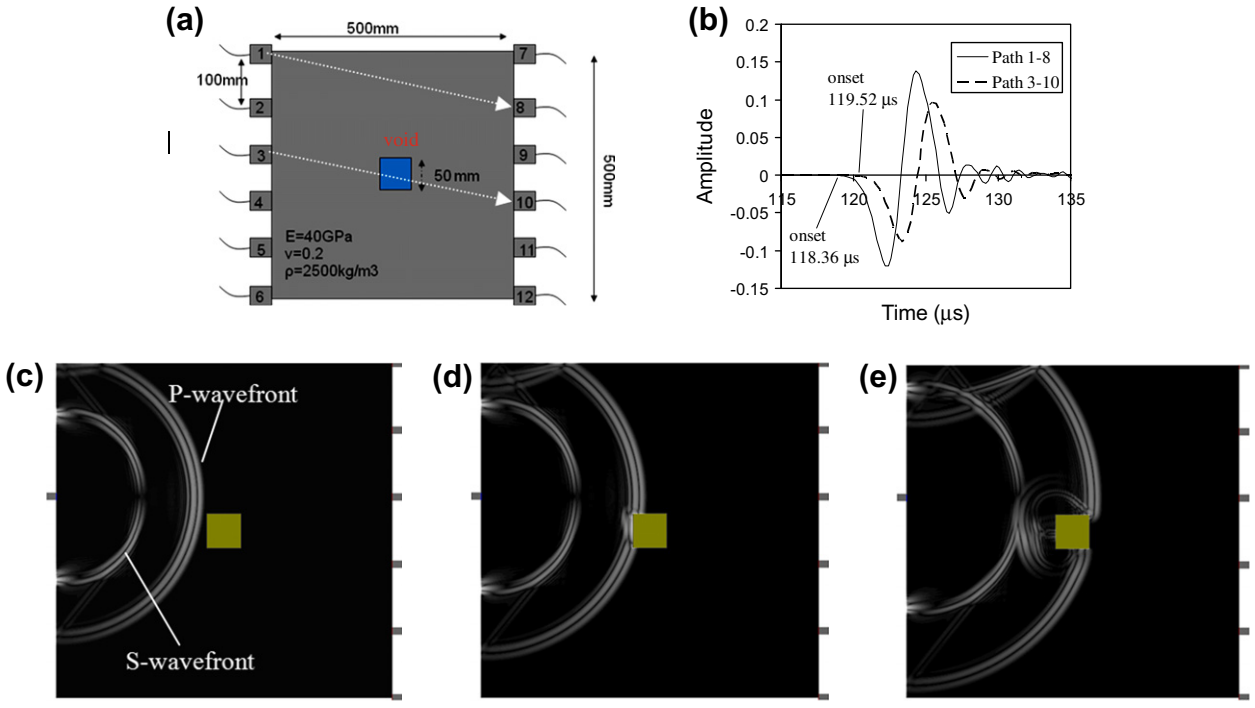

Fig. 3. Model geometry with square void, (b) simulated waveforms concerning the paths 1 → 8 and 3 → 10, (c)–(e) consecutive snapshots of the displacement field for excitation at position 3.

study. Concerning time sampling, the step was 0.05563 μs while the basic period of the highest frequency (200 kHz) was 5 μs, meaning that a typical cycle was represented by almost 100 points, while 10–20 points are considered adequate [12].

4. Tomograms

The tomograms were based on the "pulse velocity" which is commonly defined by the first detectable disturbance of the received waveform. The distance between the pulser and the receiver over the arrival time of this point leads to the pulse velocity corresponding to the specific path. The spacing between two adjacent receivers was 100 mm. In tomography reconstruction, models consisting of square elements of 50 mm and 100 mm were employed. The specific examined geometries along with the corresponding tomograms are discussed below.

4.1. Case of central void

The first case concerns a square cross section of 500 mm of concrete with a square void of 50 mm in the center, as depicted in Fig. 3a. The matrix geometry is considered to be concrete (*P*-wave velocity, C_p = 4210 m/s), while the void is air (C_p = 300 m/s). The excitation was driven consequently to 12 different positions on both vertical sides (100 mm step) and each time the sensors at the opposite side acted as receivers. For example, after excitation at position 1, the pulse transit times to positions 7–12 were recorded. Next, the excitation was conducted in position 2, while again receivers 7–12 recorded the response. It is reasonable that when the void is included on the straight line between the excitation and receiver position, the travel time becomes longer since the shortest path (straight) is not available for the wave to propagate. As an example, the waveforms collected for paths 1–8 and 3–10 are depicted in Fig. 3b. Although the distance between pulser and receiver is nominally the same for both cases (502.49 mm), the

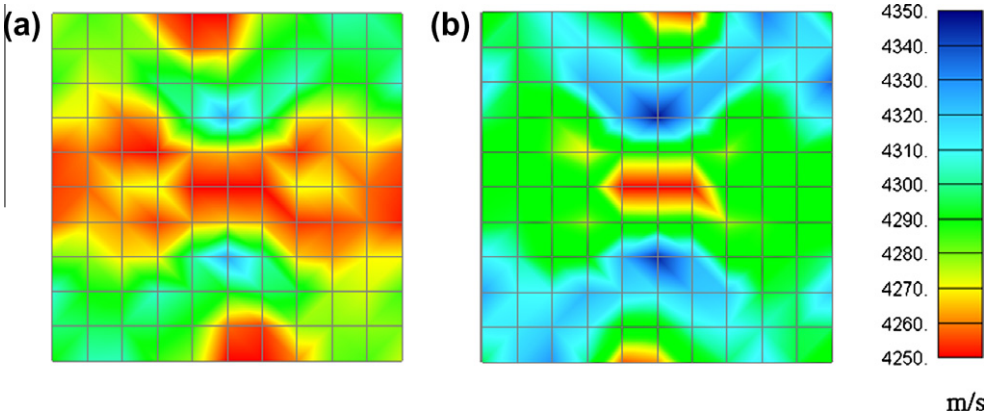

Fig. 4. Pulse velocity tomograms for the model of Fig. 3a for excitation frequency of: (a) 20 kHz and (b) 200 kHz.

Please cite this article in press as: Aggelis DG et al. Numerical simulation of elastic waves for visualization of defects. Constr Build Mater (2010), doi:10.1016/j.conbuildmat.2010.08.008

transit time differs by 1.16 μs, leading to different calculated velocities. Fig. 3c–e shows the displacement field approximately 52–70 μs after excitation at position 3 for the case of a square void (Fig. 3a). Initially the *P*- and *S*-undisturbed wavefronts can be distinguished. When *P*-wave impinges on the boundary of the square void, the wavefront is no longer uniform and the wave propagates on the surface of the void. This takes an additional amount of time resulting in lower measured velocity for the paths including the void.

The transit times for all the different pairs of pulsers and receivers (totally 72) are fed to the tomography software [16] in order to produce the corresponding tomogram. The results are shown in Fig. 4a and b for the 20 kHz and the 200 kHz excitation. In the case of 20 kHz the void causes a large fingerprint on the tomogram, much larger than its actual size, which extends through the whole section. Additionally, two other small areas of low velocity are identified on the top and the bottom of the tomograms. This however, is a normal numerical artifact due to the reduced number of wave paths passing through the corresponding top and bottom cells [16] and is not present in case the receivers are placed on all four sides, as will be seen later. The tomogram is much clearer for the case of high frequency (Fig. 4b). The area with the minimum velocity is concentrated in the center giving a more accurate depiction of the actual void. The top and bottom artifacts are still present but now in much smaller size. It is mentioned that the central area corresponding to the void is assigned a velocity near the bottom of the color scale (namely 4250 m/s), although the actual void exhibits negligible velocity (300 m/s). However, this is perfectly reasonable since the wave propagates around the void through the stiff matrix and not through. In any case the inhomogeneity can be certainly identified.

The case of circular void was also examined leading to the tomograms of Fig. 5a for the case of 200 kHz. Despite that the main dimension of the voids is equal (50 mm side for the square and 50 mm diameter for the circular one), the square void is larger in terms of surface area (2500 mm^2 while 1962 mm^2 for the circular). Although this difference of 538 mm^2 seems minimal compared to the surface area of the whole cross section (250,000 mm^2), tomography successfully captures the difference, visualizing the circular void by a smaller fingerprint than the square, as shown in Fig. 5b. The circular void is shown smaller than the square and this is due to the reduced perimeter that the wave has to propagate around the void. It is understood therefore, that even slight differences in size and shape of the defects leave a fingerprint on the tomogram.

4.2. Case of distributed deterioration

The cases simulated above are characterized by a specific void. Therefore, the transit time between specific pairs of transducers, is longer due to the presence of the void, while other paths are not influenced, leading to the small but distinct differences on the tomogram. The next case however, concerns distributed surface deterioration (see Fig. 6a) which is typical in massive structures. Any environmental deteriorative action like rain, corrosive agents, as well as thermal cycles are certainly more severe on the surface than the interior of the structure. Additionally when the structure is a part of water intake facility (dam) both sides are in contact with water. Therefore, the surface layer of old structures is more deteriorated and the damage is not uniform through the thickness. This could pose additional difficulties concerning tomography, because all the wave paths include a part of healthy concrete (center) and a part of the deteriorated surface layer. Thus, the effectiveness of tomography is challenged. The geometric model consists of a square of 500 mm similarly to the previous case, but on the left and right vertical zones of thickness 100 mm lower mechanical properties were assigned in order to simulate aging concrete (pulse velocity of 3330 m/s). The corresponding tomograms for 200 and 20 kHz are shown in Fig. 6b and c. The tomogram of 200 kHz (Fig. 6b) depicts the central area with higher velocity, successfully capturing the geometric succession of deteriotated-sound–deteriorated material on the horizontal direction, excluding the top and bottom sides which are again influenced by the reduced number of wave paths. Although the basic geometry is visualized after tomography, the velocities do not correspond to the originally set. The velocity range of the tomogram is between 3760 and 3960 m/s, while the assigned velocities for deteriorated and intact concrete are 3300 and 4200 m/s respectively. The velocities are not precise since each one of the wave paths contains a portion of healthy and two portions of deteriorated material. Therefore, there is neither a path characterized by the velocity of the sound, nor by the velocity of damaged, leading to smaller differences in the color map. The top and bottom areas with the reduced density of paths still exist, and pose certain difficulties in the explanation of the tomograms. In this case also, the frequency of 200 kHz seems to provide better characterization capacity than 20 kHz which is shown in Fig. 6c, in which the zones of different properties are not clearly depicted.

4.3. Case of distributed deterioration with embedded void

In order to estimate the visualization power for a defect hidden inside the structure between the two zones of deterioration, the

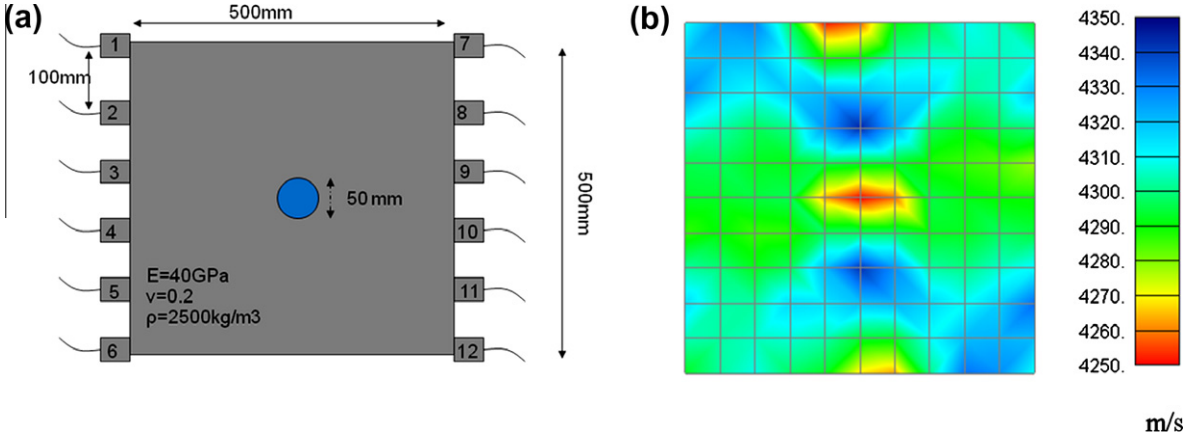

Fig. 5. (a) Model geometry with circular void, (b) corresponding tomogram for frequency of 200 kHz.

Please cite this article in press as: Aggelis DG et al. Numerical simulation of elastic waves for visualization of defects. Constr Build Mater (2010), doi:10.1016/j.conbuildmat.2010.08.008

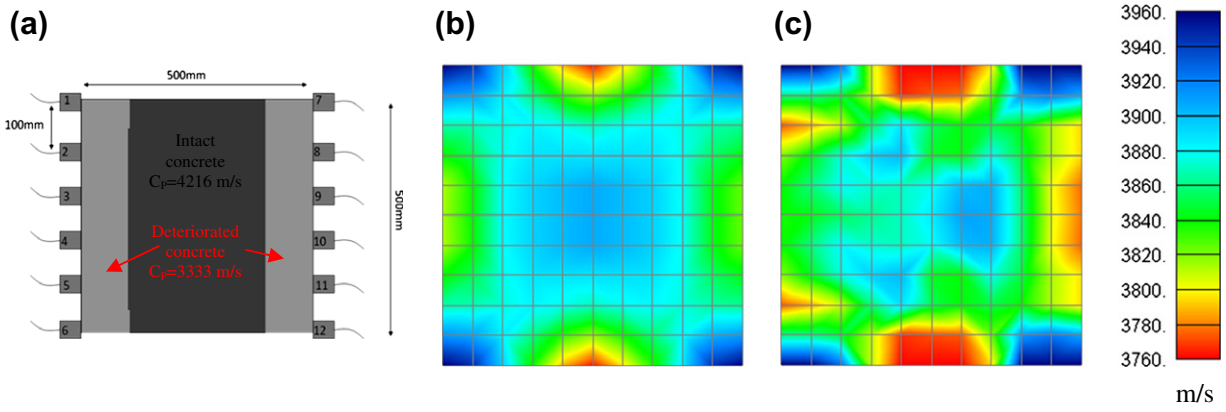

Fig. 6. (a) Model geometry with two vertical zones of deteriorated material. Corresponding pulse velocity tomograms for excitation frequency of (b) 200 kHz and (c) 20 kHz.

above case was repeated with a spherical void in the center, as shown in Fig. 7a. The results show that pulse velocity tomography is still capable of identifying the embedded void, though the change of velocity is very low and would indicate an area of the material similar to the deteriorated surface zone instead of an actual void. From the above case it is concluded that surface deterioration cannot completely mask the defects inside the structure but certainly reduces the accuracy and therefore, more detailed investigation should take place in case a fingerprint of different velocity is seen in the interior of a matrix.

4.4. Access to all sides of the cross section

The case of surface deterioration with the embedded void was again simulated using 24 transducers, thus applying excitation and reception of the wave not only from the left and right sides but also from top and bottom. The configuration is shown in Fig. 8a and the resulting tomograms in Fig. 8b and c. Now the tomograms are much clearer, adequately presenting the depth of the deteriorated zone. Moreover, the velocities of the distinct phases are more accurately calculated (3500 m/s for the deteriorated concrete). The improvement should be attributed to the fact that in this case, some of the vertical paths propagate solely through the deteriorated material, while others pass through solely healthy material; therefore, the minimum and maximum velocities are correctly set by the travel times of various paths. However, the presence of the internal void is not highlighted because it imposes only a slight deflection of the wave corresponding to a decrease of less than 100 m/s, similarly to Figs. 4 and 5. Therefore, in the range between 3500 and 4500 m/s it is barely seen. It could be highlighted only if the range is adjusted to contain velocities around 4000 m/s. In this case the slight effect of frequency is hardly visible probably because the two material zones exhibit a clear difference in pulse velocities between the distinct material zones.

4.5. Effect of steel reinforcing bar

As the inhomogeneity of the cross section increases, so does the possibility that the tomogram will not indicate the actual internal void. A possible complication is due to steel reinforcement which allows the propagation with higher velocity acting as a sort of waveguide. If metal reinforcement is present, the wave propagates through a stiffer material and therefore, any internal damage would have small or even no influence on the wave. In order to examine this case, the above geometries were reinforced by horizontal steel bars, as seen in Fig. 9a. The steel bars were simulated by rectangles of 16 mm thickness which is a typical thickness for steel reinforcing bars in concrete structures. The pulse velocity of the material of the rods was 6023 m/s to realistically simulate steel, as seen in Table 1. The bars were parallel with a vertical distance of 100 mm (see Fig. 9a). The tomograms which are included in Fig. 9b and c for the two applied frequencies show that despite the presence of the reinforcing bars, the deteriorated surface zones are still identified, even with an irregular thickness.

A small modification of this geometry, was also examined, in which the steel bars were placed exactly on the same height with each horizontal pulser–receiver line (Fig. 10a). This way, the pulse is immediately "picked" by the stiff steel material and does not

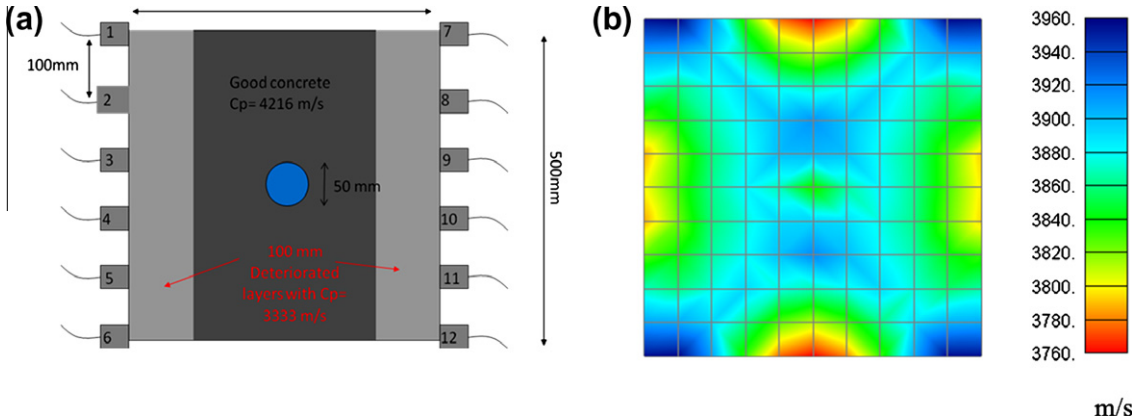

Fig. 7. (a) Model geometry with two vertical zones of deteriorated material and a circular void and (b) corresponding tomogram for frequency of 200 kHz.

Please cite this article in press as: Aggelis DG et al. Numerical simulation of elastic waves for visualization of defects. Constr Build Mater (2010), doi:10.1016/j.conbuildmat.2010.08.008

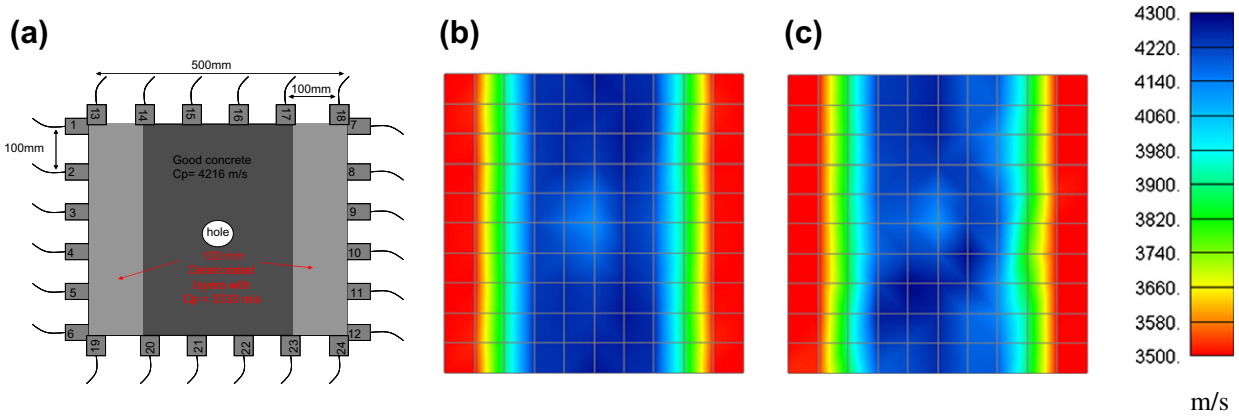

Fig. 8. (a) Model geometry with two vertical zones of deteriorated material, a circular void and four-side access. Corresponding velocity tomograms for the model of (a) for excitation frequency of (a) 200 kHz and (b) 20 kHz.

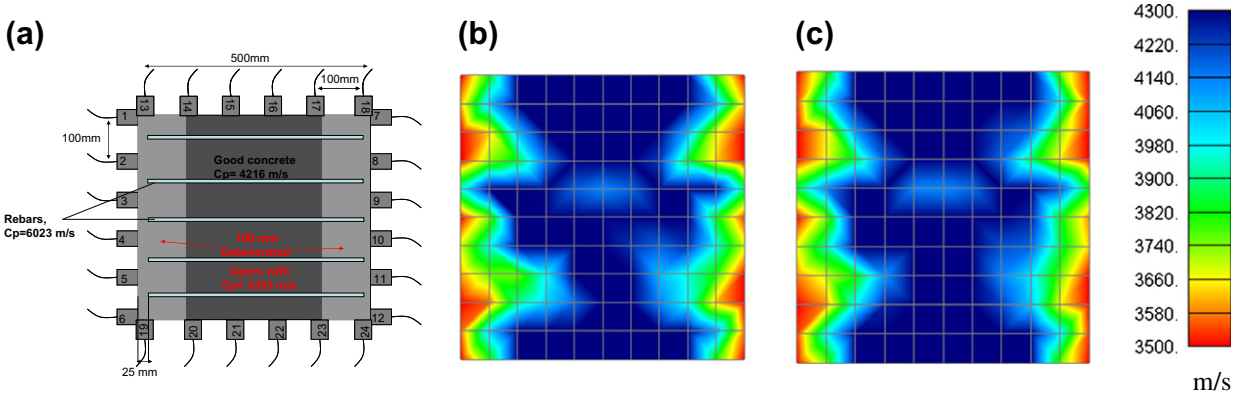

Fig. 9. (a) Model geometry with two vertical zones of deteriorated material and five horizontal steel bars with four-side access. Corresponding velocity tomograms for excitation frequency of (a) 200 kHz and (b) 20 kHz.

propagate at all through the deteriorated material zone. This can be seen on the snapshots of the displacement field of Fig. 10b and c. The stiffness of the steel bar allows the ultrasonic pulse to propagate through in a much shorter time, compared to propagation through concrete. Considering the horizontal paths, propagation takes place almost completely through the steel bars exhibiting a transit time of 88.7 μs, which is much shorter than the corresponding time in plain concrete (118.8 μs). However, the diagonal and vertical paths include less of the metal material and more of the deteriorated concrete and thus they are characterized by lower velocities, enabling tomography to capture a difference of almost 800 m/s and provide the information on the deteriorated surface, see Fig. 10d and e for 200 and 20 kHz respectively. At this point the importance of taking multiple measurements is highlighted, since one measurement can be misleading (e.g. a horizontal path as depicted in Fig. 10b and c). However, examining a network of wave paths at different directions eliminates this error and produces a tomogram that roughly represents the defective areas at both sides.

5. Discussion

Using the above configuration it was possible to obtain tomograms for some indicative geometric cases of inhomogeneous materials. At this point it is deemed essential to discuss on specific aspects of the whole procedure.

The procedure is quite sensitive to the existence of the deteriorated material zone of thickness 100 mm or a central void of 50 mm diameter. The sensitivity to the inhomogeneity size that can be characterized is largely defined by the sensor placement, as well as the tomography element size. In the present case, the distance between neighbouring measurement points is 100 mm, while the tomography cell size is set to 50 mm. This is the reason why there is no evidence of the steel bars (small thickness of 16 mm) despite their strong properties mismatch with the surrounding concrete.

In case larger tomography cell is applied (100 mm, similar to the adjacent sensors' distance) results are not changed much, but become more coarse. Fig. 11a and b concern the geometry of Fig. 8a with the surface deterioration and the central void and exactly the same input data of transit time. The difference is only the tomography cell size which in this case is 100 mm instead of 50 mm. In this case the cell size does not seem crucial probably because the dimensions of the vertical deteriorated zones are much larger than the cell size; however concerning the small circular void of Fig. 8a, which left a small but not negligible hint on the tomograms of Fig. 8b and c, in this case it does not produce even a slight visible discrepancy at that location, see Fig. 11a and b for 200 and 20 kHz respectively.

Other cases concerning the larger cell size (100 mm) can be seen in Fig. 12 for the case of steel bars in the cross section. The tomograms of Fig. 12a and b correspond to the geometry of Fig. 9a, while Fig. 12c and d to the geometry of Fig. 10a. In all cases, lower velocity is assigned to the surface, due to the simulated deteriorated zone, but the results are in a more rough form, compared to Figs. 9 and 10 with the smaller mesh size (50 mm).

Please cite this article in press as: Aggelis DG et al. Numerical simulation of elastic waves for visualization of defects. Constr Build Mater (2010), doi:10.1016/j.conbuildmat.2010.08.008

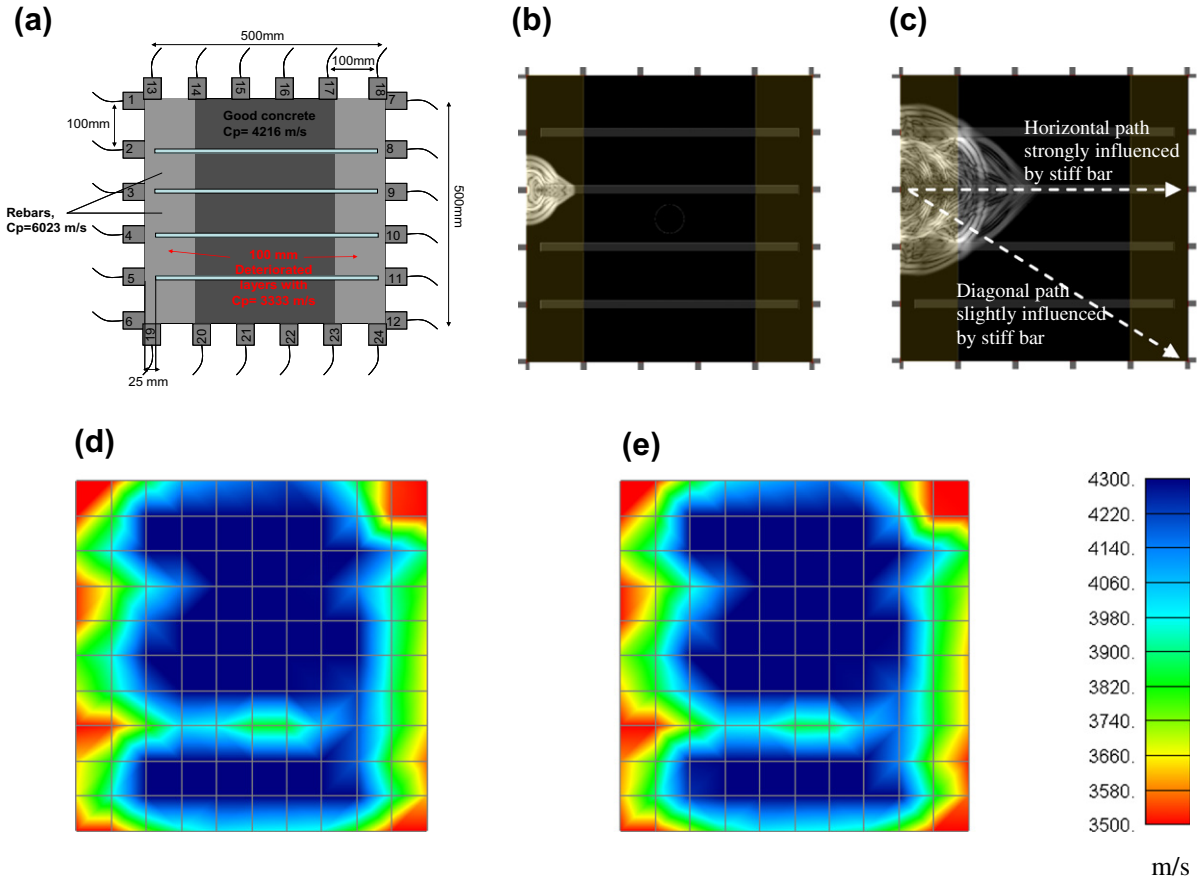

Fig. 10. (a) Model geometry with two vertical zones of deteriorated material and four horizontal steel bars with four-side access (b and c) snapshots of the displacement field after excitation at position 3 (d and e) corresponding velocity tomograms for excitation frequency of (a) 200 kHz and (b) 20 kHz.

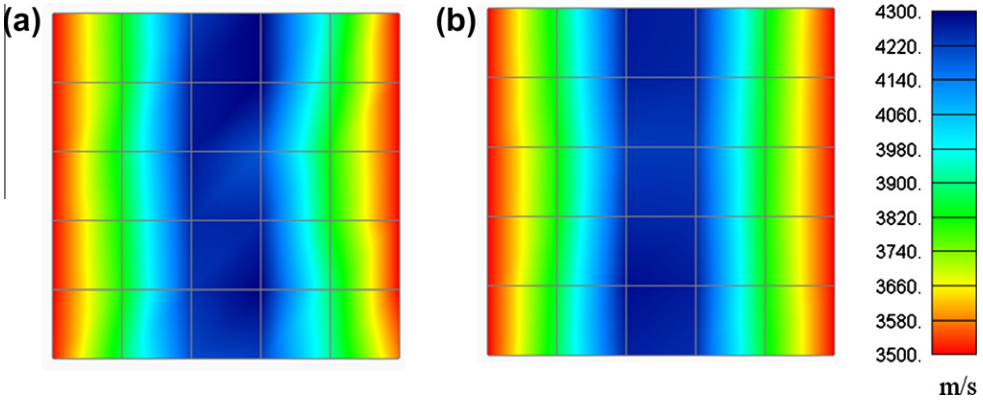

Fig. 11. Pulse velocity tomograms for the geometry of Fig. 8a for excitation frequency: (a) 200 kHz and (b) 20 kHz using element size of 100 mm.

The above shows that without changing the raw information (number of wave paths examined or number of sensors placed in the field) the results can be improved by selecting a smaller tomography mesh size. This cell could be set even to a value smaller than the distance between adjacent sensors (half in the present study). Even the slightest improvement on the quality of the tomogram, is beneficial, since it does not alter the experimental procedure which in any case is the most tiresome and time-consuming task in the monitoring of a large structure. The longer computational time taken for the tomography software to complete the necessary iterations for the larger number of nodes of a reduced mesh size is insignificant compared to a better understanding of the internal situation of a structure, while it can be overcome by the computational power of the computer used.

Concerning the wavelength/void size ratio (λ/r) it is mentioned that the applied frequencies result in ratios both higher and lower than unity. Specifically, for the frequency of 200 kHz the wavelength is 21 mm which is smaller than the typical void size applied (50 mm) resulting in a λ/r of 0.42. For the case of 20 kHz, (wavelength 210 mm) λ/r is 4.2. Although the ratios are quite different, for both frequencies damage could be identified either in the form of a central void (Figs. 4 and 5) as well as in the form of surface deterioration (Figs. 8 and 9). Therefore, a broad band of frequencies may prove suitable even if the wavelength is longer than the typ-

Please cite this article in press as: Aggelis DG et al. Numerical simulation of elastic waves for visualization of defects. Constr Build Mater (2010), doi:10.1016/j.conbuildmat.2010.08.008

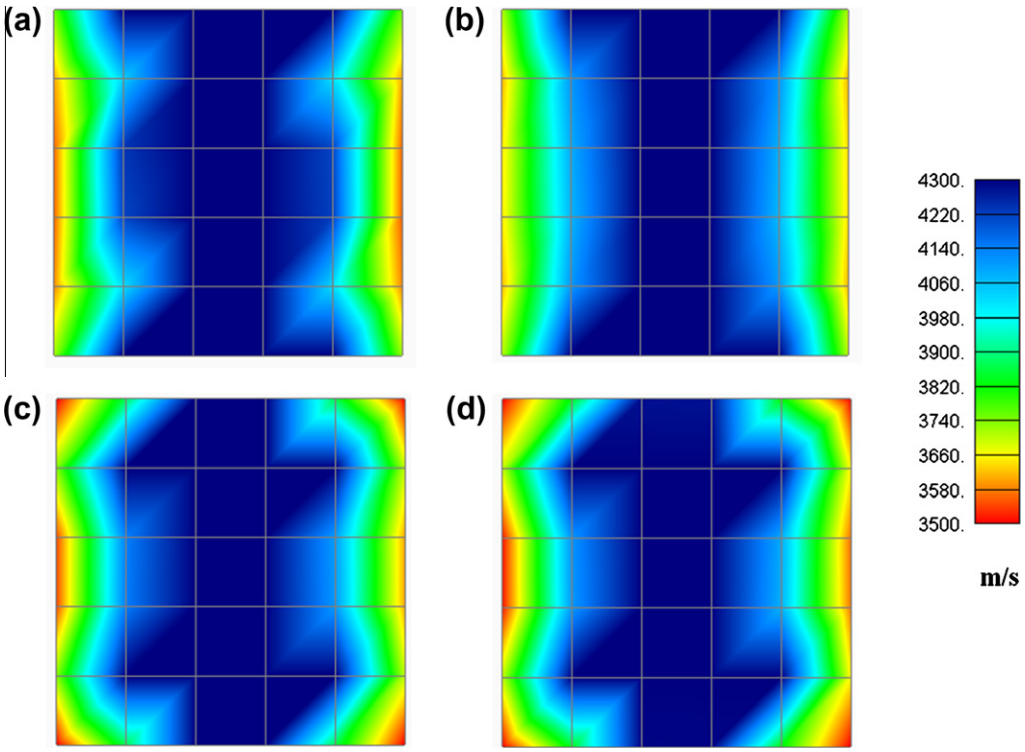

Fig. 12. Pulse velocity tomograms for the geometry of Fig. 9a with element size of 100 mm for excitation frequency: (a) 200 kHz and (b) 20 kHz. Corresponding tomograms for the geometry of Fig. 10a, with element size of 100 mm for excitation frequency: (a) 200 kHz and (b) 20 kHz.

ical size of the defect. This is important for practical cases when there are serious attenuation concerns. However, higher frequencies offer better capability since the tomograms resemble more closely the actual defects.

Another point concerns the two-dimensional (2-D) tomography analysis. It should be kept in mind that although large structures are three-dimensional, most of the tomography cases described in literature concern two dimensions, based on placement of the sensors on a cross section. In order to examine a large part of the structure's volume, the sensors' array is translated on a different 2-D cross section. The reason is mainly practical since examination of the structure in a single 3-D monitoring effort, would necessitate covering large surface areas with a huge number of sensors. Additionally, the software for 2-D tomography is much simpler and the computation time shorter.

Concerning the simulation model, 2-D simulation is a fast and economic approximation of the actual 3-D geometries. In the actual experimental case, after the wave beam impinges perpendicularly on a reinforcing bar, a part will go through the stiff steel bar. This component will travel faster and will arrive earlier to the receiver. The wave velocity will be measured by this component, because it causes the first disturbance on the receiver's surface. Any other wave component will have no influence on the measurement of pulse velocity. In the 2-D plane strain simulation, the other com-

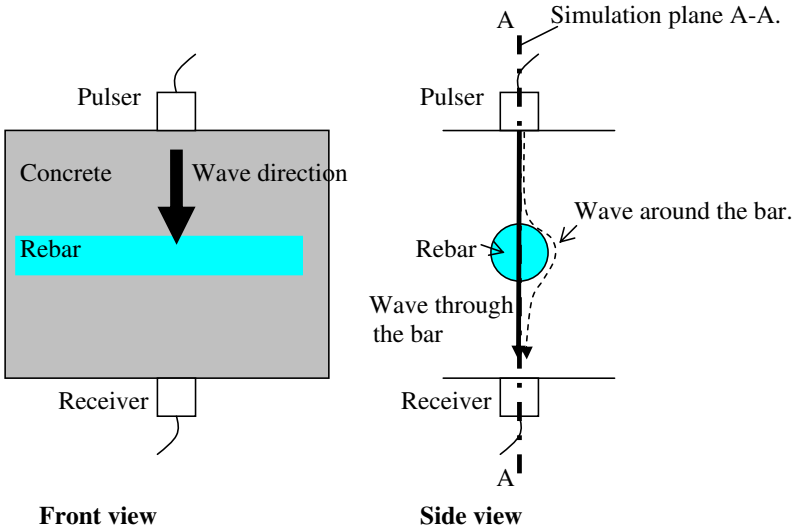

Fig. 13. Wave propagation in concrete with steel reinforcing bar.

Please cite this article in press as: Aggelis DG et al. Numerical simulation of elastic waves for visualization of defects. Constr Build Mater (2010), doi:10.1016/j.conbuildmat.2010.08.008

ponents are anyway disregarded, so this does not have any significant influence on the measurement of velocity (see Fig. 13, side view). On the other hand, 2-D simulation possibly overestimates the amplitude of the waves, since spreading of the wave beam takes place only in two dimensions, while in actual conditions, the wave would be more effectively attenuated in 3-D space. However, the transit time of the pulse is not affected.

6. Conclusion

In the present paper elastic wave propagation in different model geometries is simulated to produce the transit times for various paths. They are supplied to a tomography procedure in order to visualize the interior. The cases examined herein are just a few compared to the vast number of geometries that can be met in practical tests. However, they can act as a guide for cases of different material zones (e.g. due to surface deterioration) or presence of metal reinforcement. The basic conclusions concern both the experiment and the algorithm and are listed below:

(1) Concerning the experiment, higher frequency produces higher quality tomograms, probably due to the reduced wavelength which is more sensitive to inhomogeneity.
(2) The increase of the number of sensors, and placement on all sides of the cross section improves the quality of the tomogram. This way a denser network of the wave paths including all possible directions is measured, reducing any inconsistency due to orientation or geometry of the embedded inhomogeneity.
(3) The same set of raw data results in more precise tomograms when the tomography element size is reduced. In this case element size equal to half of the sensors separation distance proved more accurate than element equal to the separation distance. This selection concerns the computational procedure and does not delay the experimental measurement at the site.
(4) Differential deterioration on the surface layer may complicate the assessment of tomography results because all wave paths include both healthy as well as deteriorated portions of the material, posing difficulties to the ray tracing algorithm. However, the sequence of the materials is correctly identified, even though with smaller velocity discrepancies between intact and deteriorated material. Testing from all sides of the structure improves the accuracy by far.
(5) Steel reinforcing bars which are common in concrete structures may complicate the assessment of the resulting tomography but cannot completely mask the effect of deterioration, which is still evident on the tomograms.
(6) Access to all four sides of the examined cross section and refinement of the tomography mesh (application of element size less than the receivers separation distance) can overcome the reduced capacity of lower frequencies. This is extremely important for in situ testing since lower frequencies are more likely to survive propagation of long distances in deteriorated concrete. However, in case the dimensions and the attenuation of the structure allow high frequency application, this will lead to more accurate results.

The cases examined in this preliminary study are just indicative. It is proposed to examine the improvement of tomography with increasing number of sensors on more model geometries, including many distributed voids as well as more realistic defects (geometries with high aspect ratio in order to resemble actual cracks). This way the orientation of the voids will also be important for the visualization. It would also be useful to upgrade to three-dimensional tomography, which also requires three-dimensional numerical simulation, in order to represent the actual conditions of the site.

References

[1] Malhotra VM, Carino NJ, editors. CRC handbook on non-destructive testing of concrete. Florida: CRC Press; 1991.
[2] Diamanti N, Giannopoulos A, Forde MC. Numerical modelling and experimental verification of GPR to investigate ring separation in brick masonry arch bridges. NDT&E Int 2008;41:354–63.
[3] Ito F, Nakahara F, Kawano R, Kang S-S, Obara Y. Visualization of failure in a pull-out test of cable bolts using X-ray CT. Construct Build Mater 2001;15:263–70.
[4] Ohtsu M, Alver N. Development of non-contact SIBIE procedure for identifying ungrouted tendon duct. NDT&E Int 2009;42:120–7.
[5] Kepler WF, Bond LJ, Frangopol DM. Improved assessment of mass concrete dams using acoustic travel time tomography, part II—application. Construct Build Mater 2000;14:147–56.
[6] Aggelis DG, Shiotani T. Repair evaluation of concrete cracks using surface and through-transmission wave measurements. Cem Concr Compos 2007;29(9):700–11.
[7] Shiotani T, Momoki S, Chai H, Aggelis DG. Elastic wave validation of large concrete structures repaired by means of cement grouting. Construct Build Mater 2009;23(7):2647–52.
[8] Ono K. Damaged concrete structures in Japan due to alkali silica reaction. Int J Cem Compos Lightweight Concr 1988;10(4):247–57.
[9] Aggelis DG, Shiotani T, Momoki S, Hirama A. Acoustic emission and ultrasound for damage characterization of concrete elements. Am Concr Inst Mater J 2009;106(6):509–14.
[10] Chai HK, Aggelis DG, Momoki S, Kobayashi Y, Shiotani T. Single-side access tomography for evaluating interior defect of concrete. Construct Build Mater, in press.
[11] Tsinopoulos SV, Verbis JT, Polyzos D. An iterative effective medium approximation for wave dispersion and attenuation predictions in particulate composites. Adv Compos Lett 2000;9(3):193–200.
[12] Moser F, Jacobs LJ, Qu J. Modeling elastic wave propagation in waveguides with finite element method. NDT&E Int 1999;32:225–34.
[13] Schechinger B, Vogel T. Acoustic emission for monitoring a reinforced concrete beam subject to four-point-bending. Construct Build Mater 2007;21(3):483–90.
[14] Aggelis DG. Numerical simulation of surface wave propagation in material with inhomogeneity: inclusion size effect. NDT&E Int 2009;42:558–63.
[15] Naik TR, Malhotra VM. The ultrasonic pulse velocity. In: Malhotra VM, Carino 542 NJ, editors. CRC handbook on nondestructive testing of concrete. Florida: CRC 543 Press; 1991. p. 169–88.
[16] Kobayashi Y, Shiotani T, Aggelis DG, Shiojiri H. Three-dimensional seismic tomography for existing concrete structures. In: Proceedings of the second international operational modal analysis conference, IOMAC 2007, vol. 2. Copenhagen April 30–May 2, 2007. p. 595–600.
[17] Sassa K. Suggested methods for seismic testing within and between boreholes. Int J Rock Mech Min Sci Geomech Abstr 1988;25(6):449–72.
[18] Gubbins D. Time series analysis and inverse theory for geophysicists. New York: Cambridge University Press; 2008.
[19] Liu L, Guo T. Seismic non-destructive testing on a reinforced concrete bridge column using tomographic imaging techniques. J Geophys Eng 2005;2:23–31.
[20] Wave2000, Cyber-Logic, Inc., NY. /<http://www.cyberlogic.org>.
[21] Kaufman JJ, Luo G, Siffert RS. Ultrasound simulation in bone. IEEE Trans Ultrason Ferroelectr Frequency Contr 2008;55(6):1205–18.

Please cite this article in press as: Aggelis DG et al. Numerical simulation of elastic waves for visualization of defects. Constr Build Mater (2010), doi:10.1016/j.conbuildmat.2010.08.008